Spin-Stabilization and Attitude Tracking of a Spacecraft Simulator using MPC

Kumardip Basak*
Department of Aerospace Engineering,IIT Kharagpur, West Bengal 721302

Vikram Kumar Saini†, Dipak Kumar Giri‡
Department of Aerospace Engineering, IIT Kanpur, India, 208016

This paper presents simulation results for spin-stabilization and attitude tracking for a spacecraft simulator. First, a proportional derivative (PD) control is implemented, results of which are later used for comparison with model predictive control (MPC). MPC problem is formulated by constraining the control torque and simulator orientation. Control torque for this system is generated by reaction wheels (RW) and control moment gyroscope (CMG), thereby, RW motor angular speed and gimbaling servo angles are constrained. Simulation results demonstrate how a low-cost computational hardware available in the market could be used for performing control maneuvers on a spacecraft simulator.

I. Introduction

A spacecraft simulator is a free-floating object on top of a very thin layer of air maintained by a spherical air bearing. It approximates the torque-free environment experienced by a spacecraft. However, the spacecraft operates in 0-g, but the simulator works in 1-g. By careful design of the simulator, we can almost ensure that center of gravity of the simulator is at exactly the center of rotation of the simulator. The spacecraft simulators are needed for experimental validation of the theoretical results obtained for various guidance, navigation, and control (GNC) strategies for different types of missions in space. The various type of missions in space are formation flying, rendezvous and docking, berthing, capturing and detumbling of uncooperative targets, assembling space station and large telescopes, on-orbit servicing, etc. New control principles for future spacecraft must be assessed experimentally, which can be readily done on these spacecraft simulator platforms. With the rise of commercial and military satellite sectors, quick prototyping and testing of potential attitude control algorithms is needed. Other necessity for spacecraft simulators is to educate and train the engineers and scientists who are going to work on execution of space missions [1–3]. Spin-stabilization is a method to maintain the pointing direction of a spacecraft. During spin- stabilization entire spacecraft rotates around a fixed axis. Most spacecrafts use spin-stabilization for all or part of their lifetime in space. Many satellites are spin-stabilized during the orbit transfer maneuvers to reduce the effect of parasite torques generated during the firing of apogee boost motor to reduce the error in pointing vector of ΔV and other satellites are spin-stabilized for their lifetime. Spin-stabilization is advantageous because it is a passive method to maintain the pointing accuracy. Due to spin-stabilization a satellite can shut down its active GNC system and keep performing the operational tasks on battery power. This is particularly useful for low resource spacecraft which have limited computational, sensing and actuation capabilities [4]. Along with spin-stabilization, attitude tracking is also required for various spacecraft missions. Therefore, to solve the spin-stabilization and attitude tracking problem simultaneously, this paper makes an attempt to utilize MPC on spacecraft simulator platform. When using model predictive control (MPC), the plant's present state is used as the initial state for a finite horizon open-loop optimal control problem. This optimization yields an optimal control sequence, and the "first control in this sequence" is then applied to the plant as the current control action. Conventional control relies on a pre-calculated control law, and this is its fundamental difference with conventional feedback control [5–7]. Spacecraft control when involves RWs as actuators, it is a known fact that RWs tend to saturate as explained below. External secular disturbance torques, such as passive gravity gradient, aerodynamic and solar forces, and active control torques from thrusters and magnetorquers, will tend to make the wheels drift toward saturation. External disturbance torques can only be countered by a careful regulation of the three-axis reaction wheel momentum. In most cases, an external torque, such as thrusters or magnetorquers, must be supplied to push the wheel speed down

*B. Tech Student, Department of Aerospace Engineering,Indian Institute of Technology, Kharagpur, 721302
†PhD student, Department of Aerospace Engineering, Indian Institute of Technology, Kanpur, India 208016.
‡Assistant Professor,Department of Aerospace Engineering, Indian Institute of Technology, Kanpur, India, 208016.

to practically zero momentum [8]. Since it is always desirable to avoid the saturation of RWs, the MPC problem is formulated as a constrained input and constrained state optimization problem. It is recognized that MPC can handle hard constraints very well, therefore, this paper presents the application of MPC algorithm to the 3-DOF dynamics of a spacecraft simulator and compare it against PD control law.

II. Simulator Platform

The spacecraft simulator bus has a circular disc made of aluminum that is connected to an annular circular section with connecting rods. The top part of the bus is supported by a hemispherical air bearing. The bottom platform consists of all the essential components of 4 Variable Speed Control Moment Gyroscopes (VSCMG) attached with a right-angle separation along the outer rim of the platform. The spin axis of each of the Reaction Wheels (RW) is tilted 30° downward from the horizontal. The corresponding gimbal axes are perpendicular to them with 60° upward from horizontal. The bottom one also contains the necessary sensors and actuators for RW motoring and gimbal action. The top platform consists of the IMU sensor and an on-board computer. Fig. 1 describes the overview of the VSCMG based spacecraft simulator platform. This design is compact as well as it provides a better flexibility for on-board mounting the spacecraft components. Following that, a summary of the simulator's major subsystems will be given.

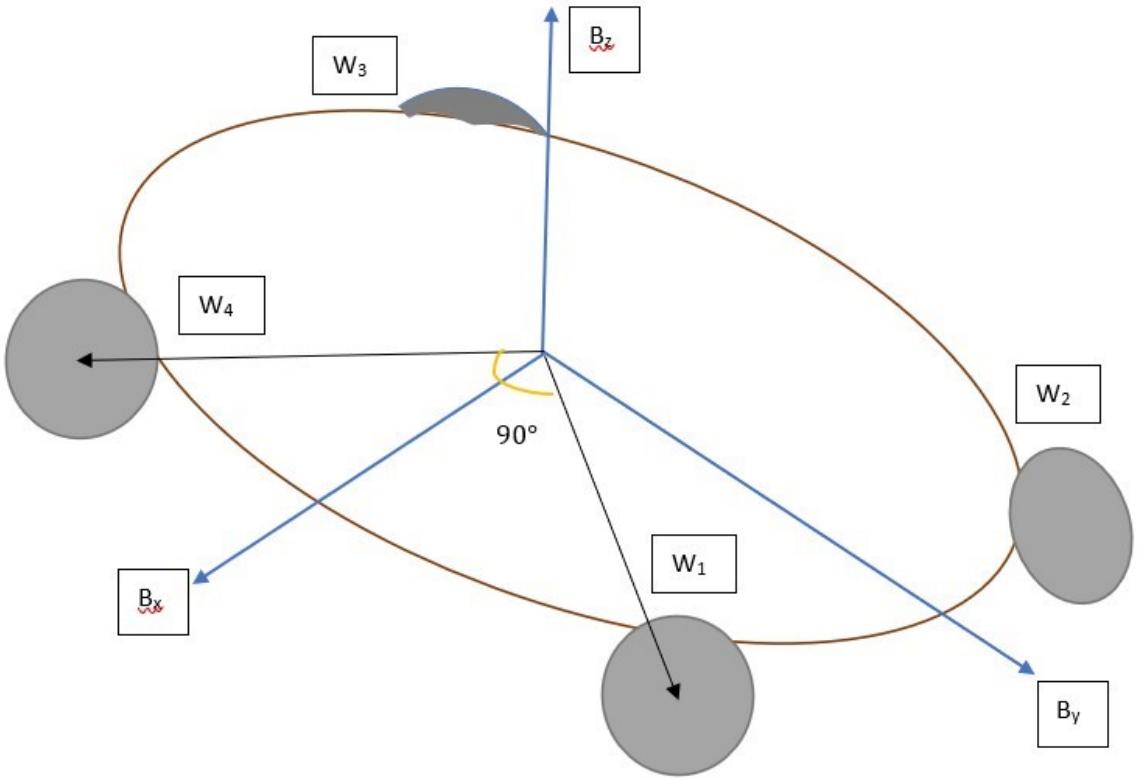

Fig. 1 Schematic of the spacecraft simulator platform with the RWs shown. The body frame axes and the RW spin axes at 0 gimbal angle is also annotated.

A. Platform and Air bearings

When compressed gas at high pressure is supplied to the air bearing, the 2-stage platform is levitated on a thin layer of air simulating frictionless movement. The air bearing is capable of ±30° angular displacement in roll and pitch about body fixed X and Y axes respectively and full rotation in yaw along Z. The placement of components on the platform is required to be perfectly balanced in order to ensure the rotation center (here, the center of the hemispherical bearing)

coincides with the center of gravity of the simulator body. This will ensure that almost zero toque is acting on the platform due to gravity. Also, by adding counterweights, the location of the center of mass can be adjusted. RW and CMG assemblies sit on the platform. The CAD model blueprint of the simulator is shown in Fig. 3.

Reaction Wheels constructed of aluminum are utilized. Four BLDC motors provide the power. There is a maximum RPM of 1200 for the RWs. Four servo motors are used for the gimbaling action of the RWs in order to achieve CMG mode. It is possible for the servos to provide an angle of rotation up to ±90 degrees with a maximum gimbal rate of 5 rad/s.

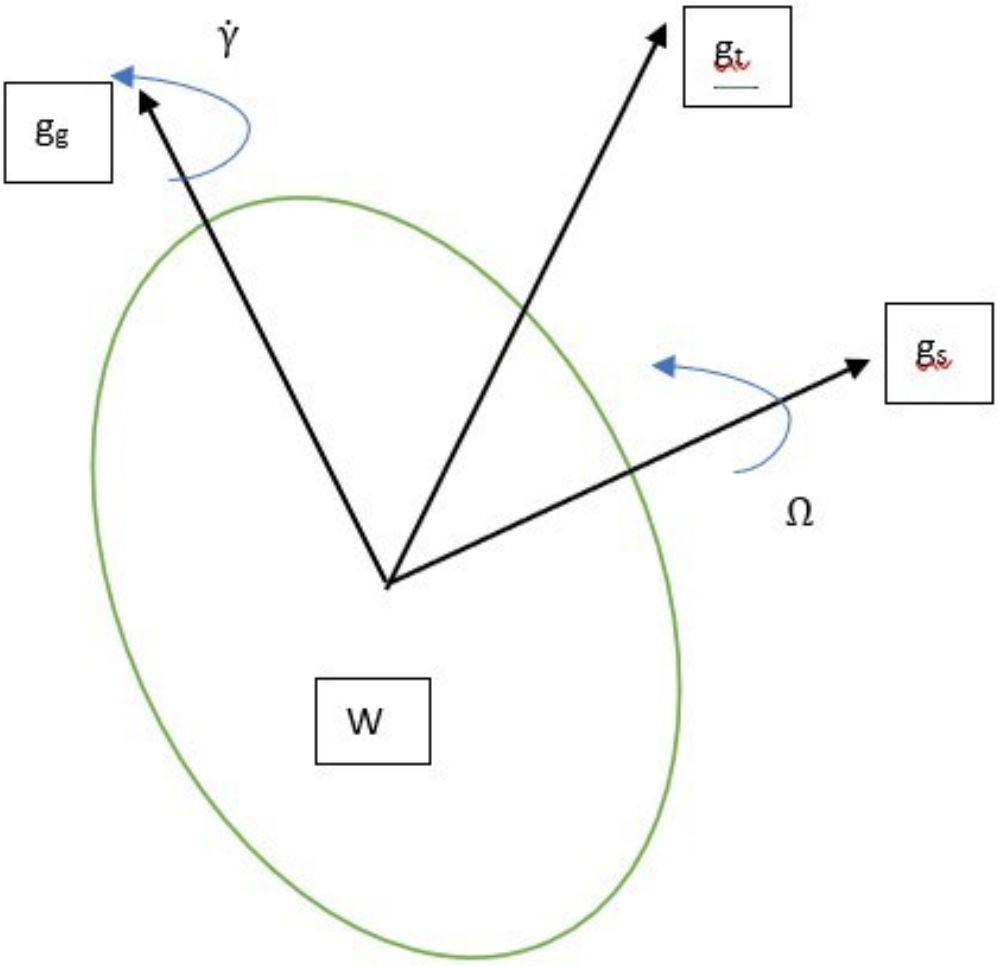

Fig. 2 Explicit RW model with spin, transverse and gimbal angle shown.

B. Sensor

Inertial Measurement Unit (IMU) and hall-effect sensors installed on BLDC motors are among the sensors on board the spacecraft simulator. The sensors that make up the IMU include accelerometers, magnetometers, and gyroscopes. Magnetometer detects the 3-axis local geomagnetic field whereas an accelerometer measures the 3-axis linear acceleration and gyroscope measures 3-axis angular rates. The Hall-effect encoder measures magnetic field variations. The spacecraft simulator's orientation and angular rate feedback are provided by fusing IMU sensors data. It is through this encoder data that the BLDC motor angular speed is determined. An analog PID controller is used to regulate the angular position of the servo motors in this experimental setup since the servos are supplied with

potentiometer feedback.

The primary structure along with the main sensors and actuators for this spacecraft simulator is described here. As the main goal for this work is to develop an optimal controller algorithm for 3DOF attitude control for this system, the furthers details of sensing, estimation, software, and other sub-components design are provided in a different article.

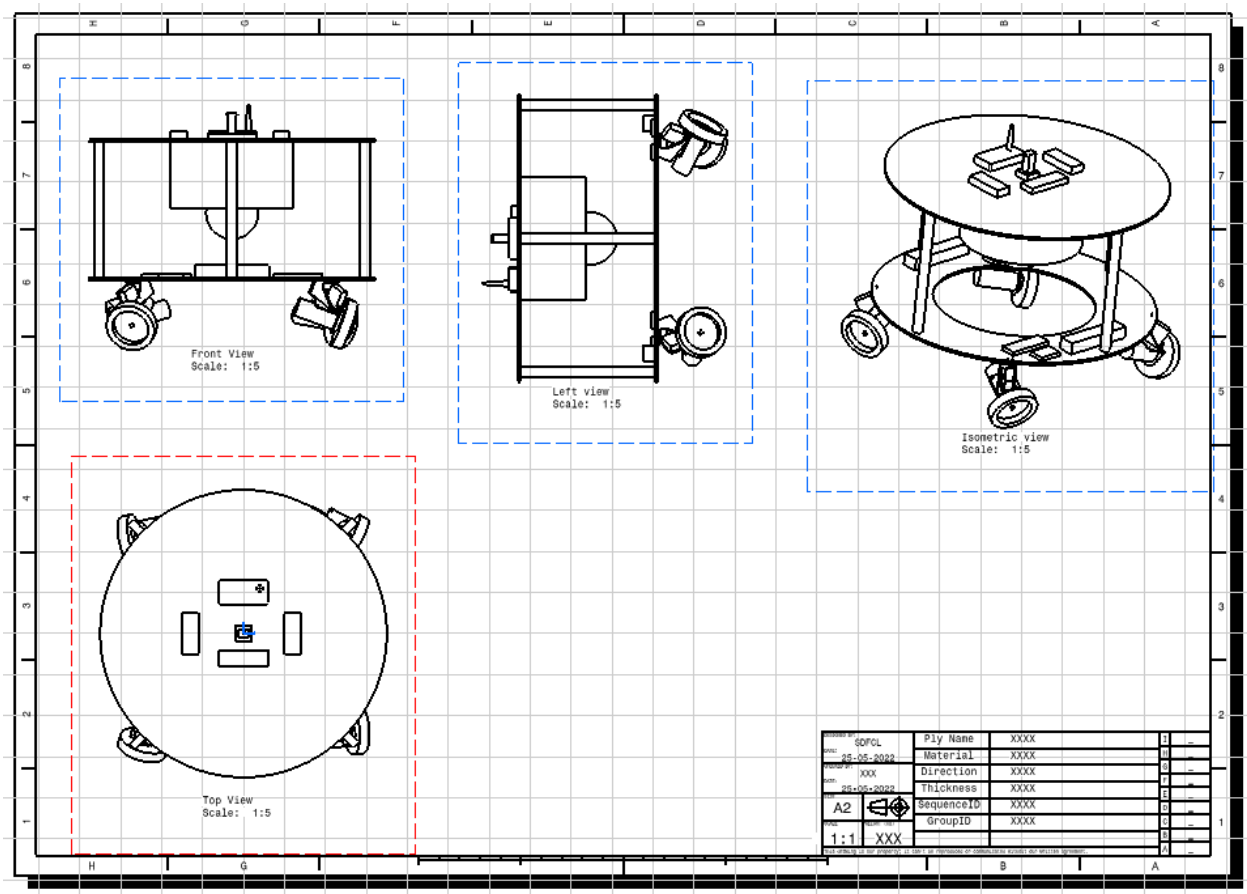

Fig. 3 Blueprint of indigenously built 3 DOF Spacecraft simulator platform.

III. Attitude Kinematics

This section talks about the reference frame that is attached to the simulator parts, how the body's attitude is shown in relation to the inertial frame, and how the attitude kinematics work.

A. Reference frames

The body reference frame lies with its X and Y axes as shown in Fig. 1. Z lies perpendicular to it. XYZ forms a right-handed coordinate system. When there is no servo rotation, the spin axes of the RWs $\hat{g}_s$ are arranged as shown. The horizontal component of the spin axes lies at 45° with respect to the body X and Y axes. Corresponding gimbal axes $\hat{g}_g$ and transverse axes $\hat{g}_t$ in right-handed fashion are shown explicitly in Fig. 2. The gimbal axes are actually fixed with respect to the body frame. The gimbal axes for the 4 servos are written as follows:

$$G_g = [\hat{g}_{g_1}, \hat{g}_{g_2}, \hat{g}_{g_3}, \hat{g}_{g_4}] \tag{1}$$

And the corresponding spin axis and transverse axis are determined using:

$$\hat{g}_{s_i} = cos(\gamma_i(t) - \gamma_{i0})\hat{g}_{s_{i0}} + sin(\gamma_i(t) - \gamma_{i0})\hat{g}_{t_{i0}} \tag{2}$$

$$\hat{g}_{t_i} = -sin(\gamma_i(t) - \gamma_{i0})\hat{g}_{s_{i0}} + cos(\gamma_i(t) - \gamma_{i0})\hat{g}_{t_{i0}} \tag{3}$$

where γ_{i_0} is the initial angular position of i^{th} servo, where i = 1,2,3,4.

B. Attitude representation

The body attitude is represented with respect to the inertial frame using Modified Rodrigues Parameter (MRP) which is an elegant method in term of attitude parameterization. MRPs (σ_i) are related to Euler Parameters (β_i) by:

$$\sigma_i = \frac{\beta}{1+\beta_0} \forall i = 1, 2, 3 \tag{4}$$

And it's related to Principal Rotation Vector (PRV) using:

$$\sigma = tan(\frac{\phi}{4})\hat{\eta} \tag{5}$$

where $\hat{\eta}$ is the principal rotation direction and ϕ is the corresponding rotation angle.

Therefore, it's clear that MRP hit singularity at principal rotation angles $\pm 360^0$. But that can be avoided by using the shadow MRP set defined by:

$$\sigma_i{}^S = \frac{-\beta_i}{1-\beta_0} \forall i = 1, 2, 3 \tag{6}$$

The MRPs are switched to shadow MRPs at the surface $\sigma^T\sigma = 1$; i.e., when the rotation angle is $\phi = \pm 180^0$, using:

$$\sigma_i{}^S = \frac{-\sigma}{\sigma^2} \tag{7}$$

Shadow MRPs are singular at 0^0. Thus, the singularity is not encountered by this switching. Direction Cosine matrix C is calculated from MRP parameters through:

$$C = I_{3\times3} + \frac{8\sigma^{\times 2} - 4(1-\sigma^2)\sigma^\times}{(1+\sigma^2)^2} \tag{8}$$

where, $S^\times$ is the cross product manipulator, given by:

$$S^\times = \begin{bmatrix} 0 & -S(3) & S(2) \\ S(3) & 0 & -S(1) \\ -S(2) & S(1) & 0 \end{bmatrix} \tag{9}$$

C. Attitude Kinematics equation

The MRP rates are related to the body angular rates through Attitude Kinematics equation, given by:

$$\dot{\sigma} = \frac{1}{4}((1-\sigma^2)I_{3\times3} + 2\sigma^\times + 2\sigma\sigma^T)\omega = \frac{1}{4}B(\sigma)\omega \tag{10}$$

It's advantageous in using this attitude representation as, the kinematics relation remains same for both MRP and shadow MRP sets.

IV. Simulator Dynamics and Equation of Motion

The dynamics is first represented with respect to one VSCMG and then extended for VSCMGs as described in the simulator design [9]. The gimbal rate about $\hat{g}_g$ axis about the body frame is given by:

$$\omega_G = \dot{\gamma}\hat{g}_g \tag{11}$$

And the spin rate of the reaction wheel about the spin axis $\hat{g}_s$ about the Gimbal frame is given by:

$$\omega_W = \dot{\Omega}\hat{g}_s \tag{12}$$

The principal moments of Inertia of gimbal axis expressed in Gimbal frame is G is $I_G = diag([I_{G_s}, I_{G_t}, I_{G_g}])$ and of the RWs written in wheel frame W is $I_W = diag([I_{W_s}, I_{W_t}, I_{W_g}])$. As the wheel is symmetrical about the spin axis $\hat{g}_s$, Wheel inertia in wheel and gimbal frame are the same. The total angular momentum of the spacecraft H with 1 VSCMG about the COM of the body is:

where,

$$H = H_B + H_G + H_W \tag{13}$$

Let, the body angular velocity with respect to the inertial frame ω is projected onto the gimbal axes system, to get the following angular rates along spin, transverse and gimbal axis as:

$$\omega_s = \hat{g}_s^T \omega \tag{14}$$

$$\omega_t = \hat{g}_t^T \omega \tag{15}$$

$$\omega_g = \hat{g}_g^T \omega \tag{16}$$

So that,

$$\omega_G = \omega_s \hat{g}_s + \omega_t \hat{g}_t + \omega_g \hat{g}_g \tag{17}$$

Now, each of the angular momentum components from Eq. 13 can be written as:

$$H_B = I_S \omega \tag{18}$$

$$H_G = I_{G_s} \omega_s \hat{g}_s + I_{G_t} \omega_t \hat{g}_t + I_{G_g} (\omega_g + \dot{\gamma}) \hat{g}_g \tag{19}$$

$$H_W = I_{W_s} (\omega_s + \Omega) \hat{g}_s + I_{W_t} \omega_t \hat{g}_t + I_{W_g} (\omega_g + \dot{\gamma}) \hat{g}_g \tag{20}$$

Next, Euler dynamical equation of motion,

$$\dot{H} = L \tag{21}$$

is applied. L is the net external torque acting on the system. The derivatives taken as initial derivatives, which are converted to body frame using vector transport theorem.

Combining the VSCMG inertia matrix as the sum of RW inertia and gimbal inertia to get $J = diag([J_s, J_t, J_g]) = I_W + I_G$. And combining that with spacecraft (without VSCMG components) inertia I_S to get the whole-body inertia matrix as $I = I_S + J$.

Therefore, the complete dynamical equation of motion of the spacecraft simulator with 1 VSCMG is derived as:

$$I\dot{\omega} = -\omega^{\times} I\omega - (J_s(\dot{\Omega} + \dot{\gamma}\omega_t) - (J_t - J_g)\dot{\gamma}\omega_t)\hat{g}_s - (J_s(\omega_s + \Omega)\dot{\gamma} - (J_t + J_g)\omega_s\dot{\gamma} + J_s\Omega\omega_g)\hat{g}_t - (J_g\ddot{\gamma} - J_s\Omega\omega_t)\hat{g}_g + L \tag{22}$$

Now, this will be extended for 4 VSCMG, where the gimbal axes lie symmetrically across the body. For multiple VSCMGs, although the spacecraft body only angular momentum rate remains constant, for the wheel and gimbal,they added up to generate net torque vectorially. The spin, transverse and gimbal axis unit vectors are compacted to 3×4 matrices like 1 as:

$$G_s = [\hat{g}_{s_1}, \hat{g}_{s_2}, \hat{g}_{s_3}, \hat{g}_{s_4}] \tag{23}$$

$$G_t = [\hat{g}_{t_1}, \hat{g}_{t_2}, \hat{g}_{t_3}, \hat{g}_{t_4}] \tag{24}$$

The total spacecraft inertia is calculated as:

$$I = I_s + \sum_{i=1}^{4} J_{s_i} \hat{g}_{s_i} \hat{g}_{s_i}^T + J_{t_i} \hat{g}_{t_i} \hat{g}_{t_i}^T + J_{g_i} \hat{g}_{g_i} \hat{g}_{g_i}^T \tag{25}$$

And the corresponding torque generating components (compact representation):

$$\tau_s = \begin{bmatrix} \dots \\ J_{s_i}(\dot{\Omega}_i + \dot{\gamma}_i\omega_{t_i}) - (J_{t_i} - J_{g_i})\dot{\gamma}_i\omega_{t_i} \\ \dots \end{bmatrix} \tag{26}$$

$$\tau_t = \begin{bmatrix} \dots \\ J_{s_i}(\Omega_i + \omega_{s_i})\dot{\gamma}_i - (J_{t_i} - J_{g_i})\dot{\gamma}_i\omega_{s_i} + J_{s_i}\Omega_i\omega_{t_i} \\ \dots \end{bmatrix} \tag{27}$$

$$\tau_g = \begin{bmatrix} \dots \\ J_{g_i}\ddot{\gamma}_i - J_{s_i}\Omega\omega_{t_i} \\ \dots \end{bmatrix} \tag{28}$$

Therefore, the net dynamical equation of motion for the spacecraft simulator with 4 VSCMGs is given by:

$$I\dot{\omega} = -\omega^{\times} I\omega - G_s\tau_s - G_t\tau_t + G_g\tau_g \tag{29}$$

The simulator dynamics with VSC,G can easily be converted to only RW mode or only CMG mode by substituting $\dot{\gamma} = 0, \ddot{\gamma} = 0$ and $\Omega = 0$ respectively.

It's important to note that, all of the vectors or matrices expressed in whatever frame must to be written in Body frame for analysis using proper DCM matrix among the two. In the next section, a stable feedback control law is implemented for the attitude regulation and tracking problem of the spacecraft simulator.

V. Nonlinear Feedback Control

In this section, a globally asymptotically stable feedback control law is implemented using proper Lyapunov function. The goal of the controller is to track a reference angular velocity ω_R. The $\sigma^R(t), \dot{\omega}^R$ are determined accordingly for the reference frame with respected to the inertial. The body frame representation of reference angular velocity and its inertial derivative is given by:

$$\omega^R{}_B = [BR]\omega^R{}_R \tag{30}$$

$$\dot{\omega}^R_B = [BR]\dot{\omega}^R_R - \omega^{\times}[BR]\omega^R{}_B \tag{31}$$

The error in angular velocity tracking is $\delta\omega_B = \omega_B - [BR]\omega^R{}_B$. Accordingly, the MRP attitude tracking error σ_r with respect to the reference is determined from attitude kinematic equation as:

$$\dot{\sigma}_r = \frac{1}{4}((1 - {\sigma_r}^2)I_{3\times3} + 2{\sigma_r}^{\times} + 2\sigma_r{\sigma_r}^T)\delta\omega \tag{32}$$

The feedback control law would target to steer the system, such that the body frame achieves $\omega_r = 0 \& \delta\omega = 0$. Hence, a radially unbounded positive definite Lyapunov function is taken as [10]:

$$V(\sigma_r, \delta\omega) = \frac{1}{2}\delta\omega^T I\delta\omega + 2Kln(1 + \sigma_r^T\sigma_r) \tag{33}$$

Therefore, the derivative of the Lyapunov function is calculated with the components taken in the body frame as:

$$\dot{V} = \delta\omega^T(I\dot{\delta\omega} + \frac{1}{2}\frac{dI}{dx}\delta\omega + K\sigma_r) \tag{34}$$

Global stability of the feedback controller is ensured by setting the derivative in Eq. 34 of the Lyapunov function in Eq. 33 as $\dot{V} = -\delta\omega^T[P]\delta\omega$, i.e., a negative semi-definite function. Although, this guarantees, only global stability of the system, higher order derivatives are calculated to prove negative definiteness and thus global asymptotic stability [10].

Thus, for the suggested Lyapunov derivative, a stability constraint for the control inputs for required control torque L_r is derived as ($\forall i = 1, 2, 3, 4$ for 4 VSCMGs):

$$D_0\dot{\Omega} + B\ddot{\gamma} + D\dot{\gamma} = L_r \tag{35}$$

where,

$$D_0 = \begin{bmatrix} \dots & J_{g_i}\ddot{\gamma}_i - J_{s_i}\Omega\omega_{t_i} & \dots \end{bmatrix} \tag{36}$$

$$D_1 = \begin{bmatrix} \dots & J_{s_i}((\Omega_i + \frac{1}{2}\omega_{s_i})\hat{g}_{t_i} + \frac{1}{2}\omega_{t_i}\hat{g}_{s_i}) & \dots \end{bmatrix} \tag{37}$$

$$D_2 = \begin{bmatrix} \dots & \frac{1}{2}J_{t_i}(\omega_{t_i}\hat{g}_{s_i} + \omega_{s_i}\hat{g}_{t_i}) & \dots \end{bmatrix} \tag{38}$$

$$D_3 = \begin{bmatrix} \dots & J_{g_i}(\omega_{t_i}\hat{g}_{s_i} - \omega_{s_i}\hat{g}_{t_i}) & \dots \end{bmatrix} \tag{39}$$

$$D_4 = \begin{bmatrix} \dots & \frac{1}{2}(J_{s_i} - J_{t_i})(\hat{g}_{s_i}\hat{g}_{t_i}^T\omega_R + \hat{g}_{t_i}\hat{g}_{s_i}^T\omega_R) & \dots \end{bmatrix} \tag{40}$$

$$B = \begin{bmatrix} \dots & \hat{g}_{g_i}J_{g_i} & \dots \end{bmatrix} \tag{41}$$

$$D = D_1 - D_2 + D_3 + D_4 \tag{42}$$

And required control torque is:

$$L_r = K\sigma_r + P\delta\omega + L - \omega^{\times}I\omega - I(\dot{\omega}_R - \omega^{\times}\omega_R) - \sum_{i=1}^{4} J_{s_i}(\Omega_i\omega_{g_i}\hat{g}_{t_i} - \Omega_i\omega_{t_i}\hat{g}_{g_i}) \tag{43}$$

It must be noted that the attitude as well as angular velocity of the system can be steered to the reference using 3 different torque generating terms: RW spin acceleration $\dot{\Omega}$, Gimbal angular rate $\dot{\gamma}$ and Gimbal angular acceleration $\ddot{\gamma}$. But, for most of the physical systems, B is smaller than D_0 and D, thus $B\ddot{\gamma}$ term can be ignored for torque generation. Thus, the required control torque L_r can be produced by $\dot{\Omega}$ and $\dot{\gamma}$ by pre-defined torque splitting. In the next section, simulations are performed for different cases using different torque splitting.

VI. MPC Control and System stability

To apply linear Model Predictive Controller (MPC), the nonlinear system has to be has to be linearized at some operating point. Then it is being discretized. The State Space model is considered is of order 3 consisting of the angular velocity errors $\delta\omega$. There are 8 inputs to the system: the RW spin rates and gimbal rates. Thus the discrete State Space model is given by:

$$X_{k+1} = A_k X_k + B_k U_k \tag{44}$$

$$Y_k = C_k X_k \tag{45}$$

where, the states and the inputs belong to their corresponding admissible set. Now, the MPC problem is defined as:

$$\min_x J_{MPC} \ni EX < b \tag{46}$$

where,

$$J_{MPC} = \left[(\overline{\boldsymbol{Y}} - \overline{\boldsymbol{Y_d}})^T \boldsymbol{Q_y} (\overline{\boldsymbol{Y}} - \overline{\boldsymbol{Y_d}})\right] + \left[(\overline{\boldsymbol{U}} - \overline{\boldsymbol{U_d}})^T \boldsymbol{Q_u} (\overline{\boldsymbol{U}} - \overline{\boldsymbol{U_d}})\right] + \left[(\overline{\boldsymbol{\Delta U_m}})^T \boldsymbol{Q_{\Delta u}} (\overline{\boldsymbol{\Delta U_m}})\right] + \text{constraint violation terms} \tag{47}$$

$$\boldsymbol{E} = \left[\boldsymbol{I}_{3\times3}^{\boldsymbol{T}} - \boldsymbol{I}_{3\times3}^{\boldsymbol{T}}\boldsymbol{L}^{\boldsymbol{T}} - \boldsymbol{L}^{\boldsymbol{T}}\boldsymbol{R}^{\boldsymbol{T}} - \boldsymbol{R}^{\boldsymbol{T}}\right]^{\boldsymbol{T}}$$

$$\boldsymbol{b} = \begin{bmatrix} \Delta\boldsymbol{U}(k)_{\max} \\ -\Delta\boldsymbol{U}(k)_{\max} \\ \boldsymbol{U}(k)_{\max} - \boldsymbol{U}(k-1) \times \text{ ones } (m,1) \\ \boldsymbol{U}(k-1) \times \text{ ones } (m,1) + \boldsymbol{U}(k)_{\max} \\ \boldsymbol{Y}(k)_{\max} \\ -\boldsymbol{Y}(k)_{\max} \end{bmatrix}$$

where, J_{MPC}, $\boldsymbol{E}$ and $\boldsymbol{b}$ are MPC cost function, constraint violation coefficient and constraint values respectively. $\boldsymbol{Q_y}$, $\boldsymbol{Q_u}$ and $\boldsymbol{Q_{\Delta u}}$ are cost weighting matrices for outputs, inputs and input-rates respectively. T_p and T_m are taken as Prediction horizon and Control horizon respectively.

A. Linear MPC stability for time invariant discrete system

In this section, the stability of MPC control for a linear time invariant in discrete time is discussed by choosing a proper Lyapunov function for the concerned system. Stability using terminal constraints is presented here, although the constraint is completely compatible with the system. Consider the system given by Eqs. 44 and 45 and model predictive controller for the plant.

Definition 1: The value of the cost function at time instant k is denoted by $N(\boldsymbol{X}_k, \boldsymbol{U}_k)$, which is represented by $N(z_k) = N_y(z_k) + N_u(z_k) + N_{\Delta u}(z_k) + N_\varepsilon(z_k)$. Then, the value of total cost function is given by $V(z_k)$, where

$$\mathrm{V}(z_k) = \sum_{i=1}^{p} N(z_k) \tag{48}$$

Theorem 1: System's equilibrium point, i.e., $X = 0$ is stable, provided the feasible optimization problem, if it is subject to the terminal constraint: $\boldsymbol{X} \mid (k+p \mid k) = 0$, where $N(\boldsymbol{X}_k, \boldsymbol{U}_k) \geq 0$ and $N(\boldsymbol{X}_k, \boldsymbol{U}_k) = 0$ if $\boldsymbol{X}_k = 0$ and $\boldsymbol{U}(0) = 0$.

Proof: If optimal value of the value function $V(\boldsymbol{X}, \boldsymbol{U})$ and the optimal input is $\boldsymbol{U}_k$ at time k is given by V^* and $\boldsymbol{U}^*$ respectively. For simplicity, $T_p = T_m = p$. With this assumption, it is written as:

$$\begin{aligned} V^*(k+1) &= \min_u \sum_{i=1}^{p} N(\boldsymbol{X}_{k+1+i}, \boldsymbol{U}_{k+i}) \\ &= \min_u \left\{ \sum_{i=1}^{p} N(\boldsymbol{X}_{k+i}, \boldsymbol{U}_{k-1+i}) - N(\boldsymbol{X}_{k+1}, \boldsymbol{U}_k) + N(\boldsymbol{X}_{k+1+p}, \boldsymbol{U}_{k+p}) \right\} \\ &\leq -N(\boldsymbol{X}_{k+1}, \boldsymbol{U}_k) + V_k + \min_u N(\boldsymbol{X}_{k+1+p}, \boldsymbol{U}_{k+p}) \end{aligned} \tag{49}$$

As the optimum $N(\boldsymbol{X}_{k+1}, \boldsymbol{U}_k)$ is no worse than keeping the optimal solution at time k. As the assumed condition $\boldsymbol{X}(k+p \mid k) = 0$ is satisfied, then the optimal input $\boldsymbol{U}(k+p \mid k) = 0$ remains at 0, with $\boldsymbol{X}_k = 0$ further. Hence, the optimization is also satisfied to get a feasible solution. This gives:

$$\min_u N(\boldsymbol{X}_{k+1+p}, \boldsymbol{U}_{k+p}) = 0 \tag{50}$$

Now, as $N(\boldsymbol{X}_{k+1+p}, \boldsymbol{U}_{k+p}) \geq 0$, then from Eq. (49), it can be shown that $V_{k+1}^* \leq V_k$. Therefore, it can be concluded that, V_k is a Lyapunov function candidate and the system is stable at $\boldsymbol{X} = 0$ and $\boldsymbol{U} = 0$.

VII. Results and Discussion

A globally asymptotically stable feedback controller for attitude tracking problem for this 4 VSCMG based spacecraft simulator is developed in this work. Accordingly, simulation results are performed considering different reference angular velocity conditions. Different torque splitting is being used among RW rate and Gimbal rate to generate the

required feedback control torque. For each case, the variation of angular velocity, relative MRP coordinates, wheel RPMs and gimbal angles with respect to time are plotted to prove the effectiveness of this method.

For the simulation, maximum wheel RPM is taken as 1200, and maximum servo angle is taken as 90° with max. gimballing rate 5 rad/s as already stated in Section III. The inertia matrix of the RW is wheel as well as in Gimbal frame is same and calculated from component specifications datasheet as $I_W = diag([9.0922e-4, 4.8326e-4, 4.8326e-4])kg.m^2$ and the same for the gimbal, here the servo motor that rotated using the servo that performs the gimballing action, is calculated as $I_G = diag([1.5188e-4, 5.7594e-4, 5.7594e-4])kg.m^2$. Therefore, the net inertia of the VSCMG components in their default position becomes $[J] = I_G + I_W$. An estimated and nearly approximate inertia matrix is calculated from the CAD model of the whole simulator as $I = diag([0.01178, 0.01178, 2 * 0.01178])kg.m^2$.

A. Case A1: Regulation Problem

The regulation problem is simpler than the tracking one. Here, the simulator body is given an initial angular velocity, where the goal of the controller is to steer it to $\sigma_r = 0$ and $\omega^R = 0$. In this simulation, the initial body angular rates are given as $\omega(t = 0) = [(-0.5, 0.1, 0.3)]rad/s$, with having zero RW spin and Gimbal angles. For the control torque splitting, 60% and 40% is set to be produced using the RW spin angular acceleration and Gimbal angular rate respectively.

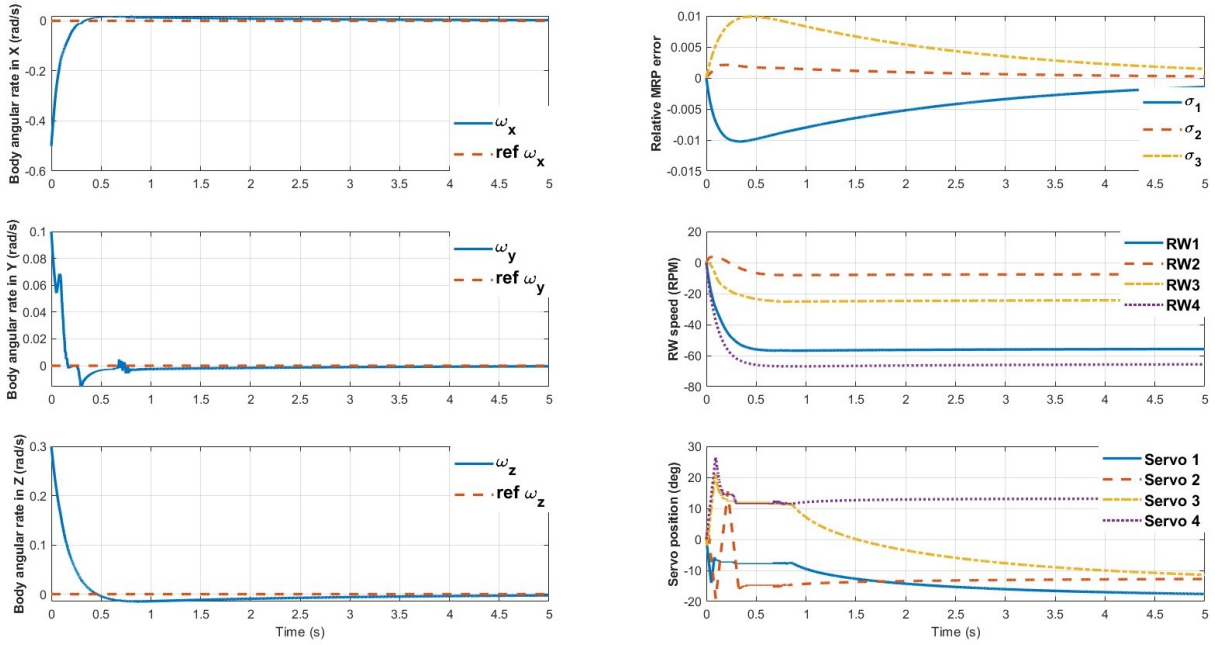

Fig. 4 Attitude regulation control with each simulation aspects plotted as mentioned in VSCMG mode using nonlinear control.

The regulation problem simulation in MATLAB and the results are presented in Fig. 4. In this simulation, an initial angular velocity is given to the body. The globally asymptotically stable feedback controller algorithm simultaneously operates 4 Reaction wheels and 4 Servos, controlling their RPM and angular position respectively, based on the commanded spin acceleration and gimbal rate. It can be seen from the results that; the body angular rates have reached the corresponding steady state with an exceedingly small tolerance limit within 4 seconds. Similarly, the relative MRP error is also tracked to 0. The RW spin rates as well as the servo positions have reached a fixed position and stayed there. In the due course of the simulation, the RWs are not saturated as well as the Servos haven't hit their maxima. The net angular momentum is conserved with the regulation control successfully performed providing a satisfactory transient and steady-state response.

B. Case A2a: Tracking Problem in VSCMG mode

In this case, the goal of the controller is to track a commanded reference angular velocity over a period of time. For this simulation, the initial body angular velocity is kept as $\omega(t=0) = [(0,0,0)]rad/s$, and having zero RW spin and Gimbal angle. The reference angular rates are given as $\omega^R = [(0.5,-0.4,0.3)]rad/s$ from $t = 0$ to 40 seconds and $\omega^R = [(0.3,-0.2,0.1)]rad/s$ from $t = 60$ to 100, else $\omega^R = 0$. The control torque splitting is kept at 50% each for RW spin acceleration and Gimbal rate.

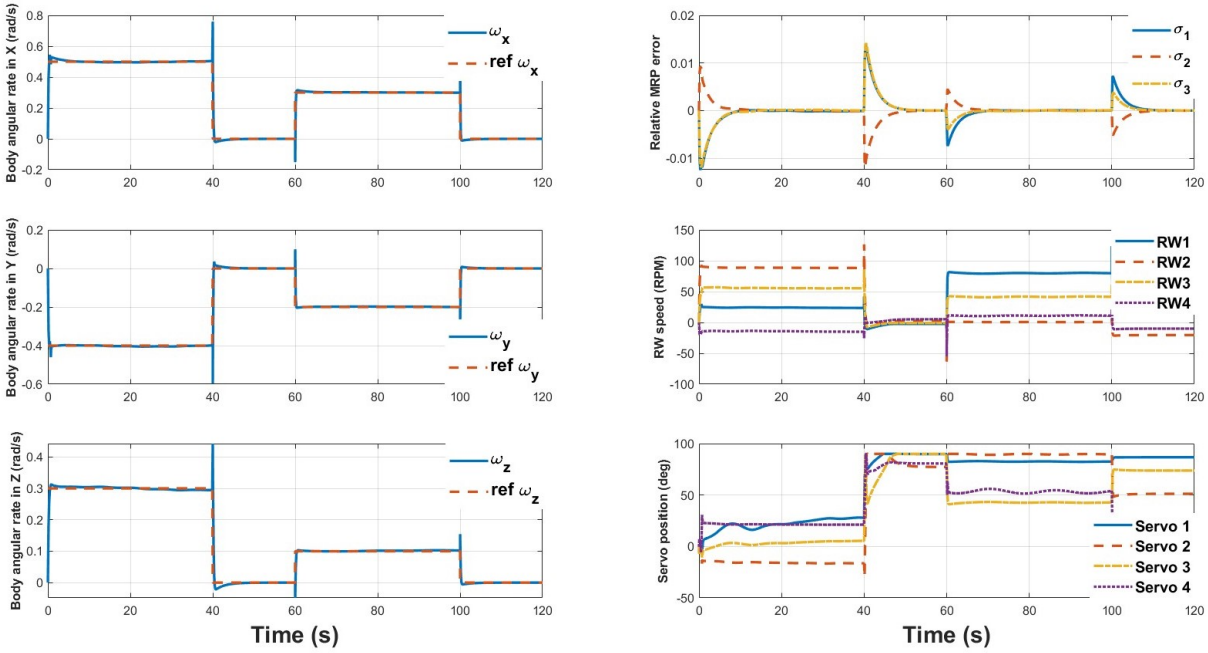

Fig. 5 Attitude tracking control with each simulation aspects plotted as mentioned in VSCMG mode using nonlinear control.

This is the first simulation done in tracking problem and the results are presented in Fig. 5. The angular velocity tracking results in all 3 axes clearly concludes a satisfactory remark for the controller with perfectly tracking the time dependent reference signal. The settling time is always within 5 seconds of reference shift. The relative MRP attitude error perfectly converges to 0, for all of the 4 sections of reference shift in the simulation. This was run in VSCMG mode with equal control torque splitting. The variation of RW spin rates and Gimbal positions are provided too. The RWs are not saturated, but the Servos seem to have reached their positive maxima in certain periods of the simulation duration.

C. Case A2b: Tracking Problem in RW mode

The initial condition for body angular rates and VSCMG components as well as the reference angular velocity commands are kept intact as of the previous case. Whereas, this case is run only in RW mode, keeping gimbal angles fixed at 0. Thus, the required control torque is totally generated using RW spin acceleration.

Fig. 6 is the second attitude tracking simulation, run exactly with same initial and reference conditions as the previous. Only, this was run in RW mode, thus the control torque is only generated using RW spin acceleration. For this case, the body angular velocity perfectly tracks the commanded with satisfactory performance. Accordingly, the attitude error is also steered to 0. The RW spin haven't saturated in simulation period with Servos fixed to 0.

The simulation results in Fig. 5 and Fig. 6 in VSCMG and RW mode respectively, points out some important information. In VSCMG mode, the maximum spin rate reached by the RW wheel is lesser than that of RW alone, which can be clearly explained that in case of VSCMG, the control torque is generated in distributed manner, thus requiring lesser spin acceleration. But the system tracking performance is better in case of RW only mode with lesser rising and settling time. Although, it is compensated by more overshoot in RW only case, compared to VSCMG mode. Another crucial observation from the simulation results is that, the spin acceleration is quite large in most of the cases, where precise attitude tracking requires exact following of the commanded RW spin rates and Servo positions. Although in

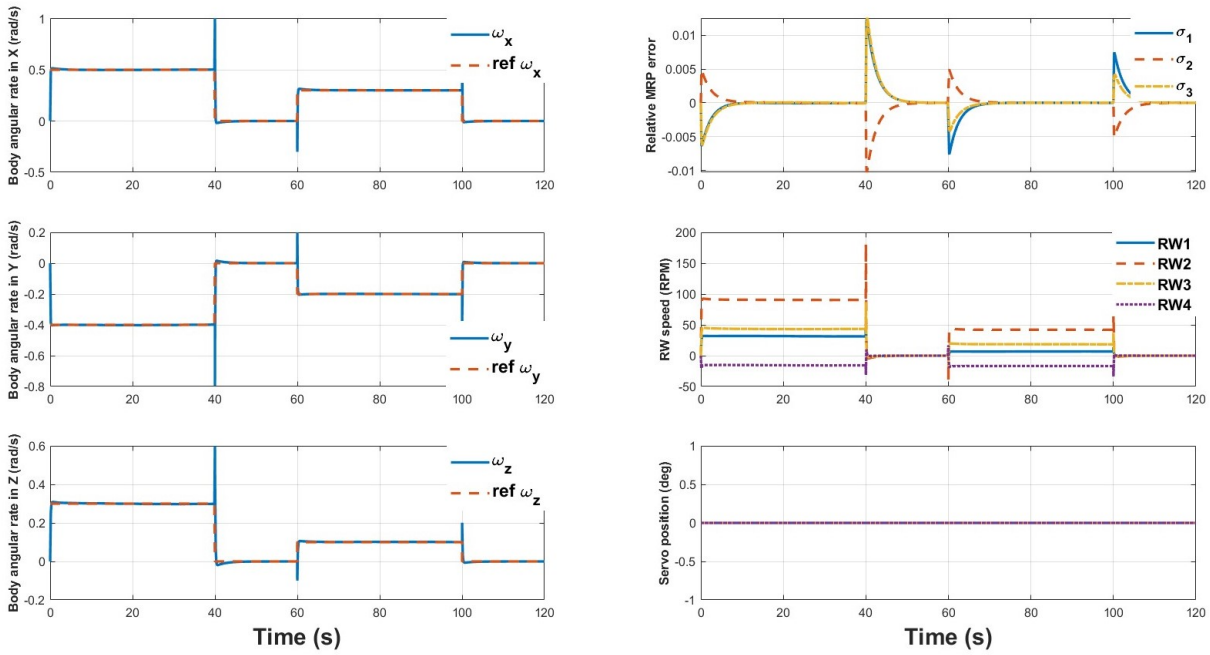

Fig. 6 Attitude regulation control with each simulation aspects plotted as mentioned in RW mode using nonlinear control.

reality, the motors and the servos used have some inherent lag in the system, that can hamper system performance. And that rapid acceleration in the system, requires much control effort, power usage and causes jerk in the system affecting spacecraft simulator electronics and other subsystems. Thus, for an optimal system performance of attitude regulation and tracking, and actuator effort with real hardware simulation, it cannot be achieved using this PD law. Therefore, need of an optimal controller is necessary.

Hence, the designed MPC controller is implemented in this purpose. The linear MPC controller for the plant, engineered for this problem is linearized about $\boldsymbol{X = 0}$ (relative angular velocity errors = 0). The prediction and the control horizon is set at 35 and 2, respectively. The sampling time of the controller is set to 0.01 second. The input and input-rate constraints were provided as $max : [40\pi, 40\pi, 40\pi, 40\pi, 5, 5, 5, 5]; min : [-40\pi, -40\pi, -40\pi, -40\pi, -5, -5, -5, -5]$ and $max : [2, 2, 2, 2, 2, 2, 2, 2]; min : [-2, -2, -2, -2, -2, -2, -2, -2]$, respectively. Corresponding weights for inputs and input-rates are given as 7 and 10, respectively. The state bound on outputs are intentionally kept at infinity. The weights on the output variables are kept 4 for relative angular velocity. Therefore, the proposed MPC controller ready to test for this attitude control motion in for the following situations.

D. Case B1: Regulation problem

The initial condition for body angular rates and VSCMG components as well as the reference angular velocity commands are kept intact as of the VII.A. The simulator is intended to stabilize at 0 angular velocity, from an initial value. Given the constraints, MPC is run for the system.

The regulation simulation results are shown in Fig. 7. The intention of the controller is to stabilize the initially rotating simulator to 0. The stable MPC controller simultaneously operates 4 Reaction wheel speeds and 4 Servo rates. The angular velocities plot verified that the body angular rates have reached the corresponding steady state within very short time. The RW spin rates as well as the servo positions have reached a fixed position and stayed there. Both RW and Servos haven't hit the saturation limits. Here, an observation must be noted that the relative MRP is fixed at a non zero level. This is due to the linearization effect of the nonlinear dynamics. The Servos have also shown no movement at all. The regulation controller successfully performed providing a satisfactory transient and steady-state response in terms of relative angular velocity.

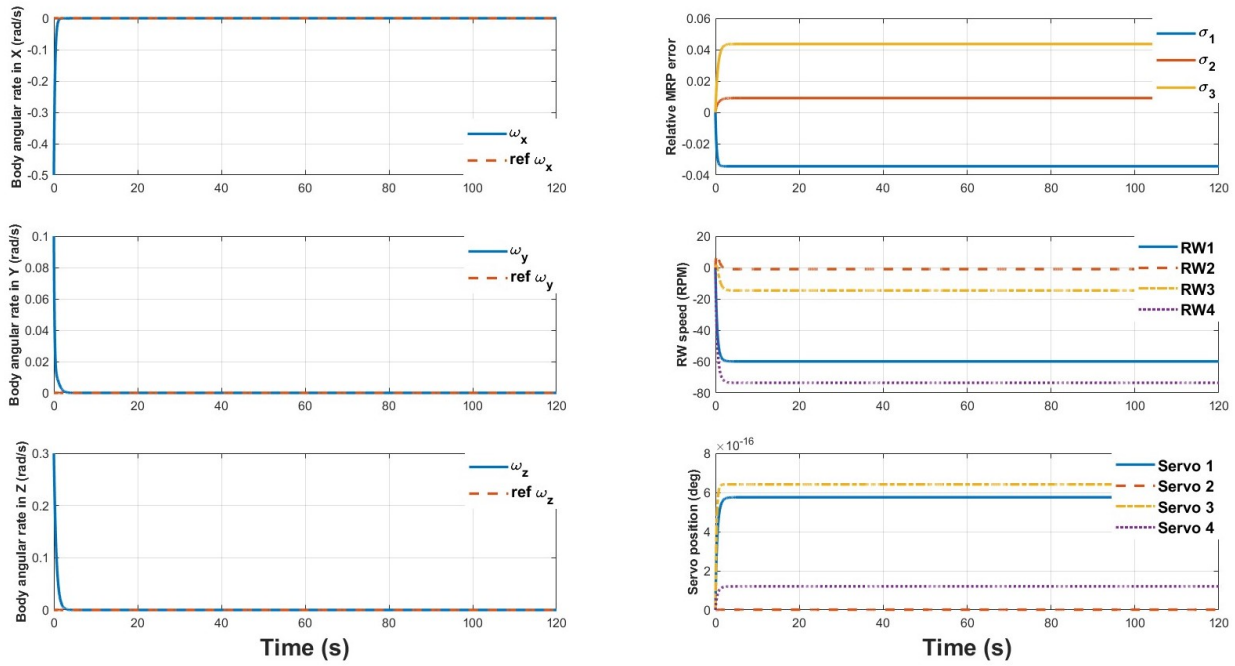

Fig. 7 Attitude regulation control with each simulation aspects plotted as mentioned in VSCMG mode using MPC control.

E. Case B2: Tracking problem

The initial condition for body angular rates and VSCMG components as well as the reference angular velocity commands are kept intact as of the VII.B. The simulator is intended to track the commanded reference angular velocities over time. Given the constraints, MPC is run for the system.

The tracking simulation results are displayed in Fig. 8. The angular velocity tracking results in all 3 axes is clearly satisfactory with the MPC tracking the time dependent reference signal. The relative MRP attitude error perfectly converges to 0, when the commanded reference is also 0 in the simulation, not in all 4 sections. This was run in VSCMG mode. The variation of RW spin rates and Gimbal positions are provided too. For this case too, the Servos are not moving at all, and the angular velocity control is done using RW only. None of the RW and Servo angle have reached their limits.

In terms of transient response, the MPC controller certainly has better response than Lyapunov function based nonlinear controller. MPc has way shorter rise time, lesser overshoot and shorter settling time than the nonlinear feedback one. The in-between transitions angular velocity as well as the actuation spikes are present in the nonlinear, which is completely mitigated using MPC, because of its constrained optimization power. These sudden rise in angular velocities or the actuation could be harmful for the system, which won't be the case using MPC. Most importantly, the power consumption. In case of nonlinear feedback control, the RWs and Servos are simultaneously actuated to stabilize or track the angular velocities with the relative MRPs going to zero. Whereas in case of MPC based controller, as it uses a linearized model, only angular velocity feedback and stabilization is possible, which is done using RWs. The magnitude of RW actuation is also slightly lesser than that of nonlinear controller, even if the Servos are not moving. Hence, during the cases of attitude stabilization, where to tracking or regulating the relative angular velocities are the primary tasks, MPC is verified to be beneficial in terms of lesser power consumption, as well as having significantly better transient state response with realistic and safe actuation inputs.

VIII. Conclusion

The control algorithm developed in the paper using MPC, has been successfully able to perform the attitude regulation and tracking control for the designed 4 VSCMG based 3 DOF spacecraft simulator. From the simulation results, it's evident that implementing MPC controller along with state and input constraints has optimal state performance and

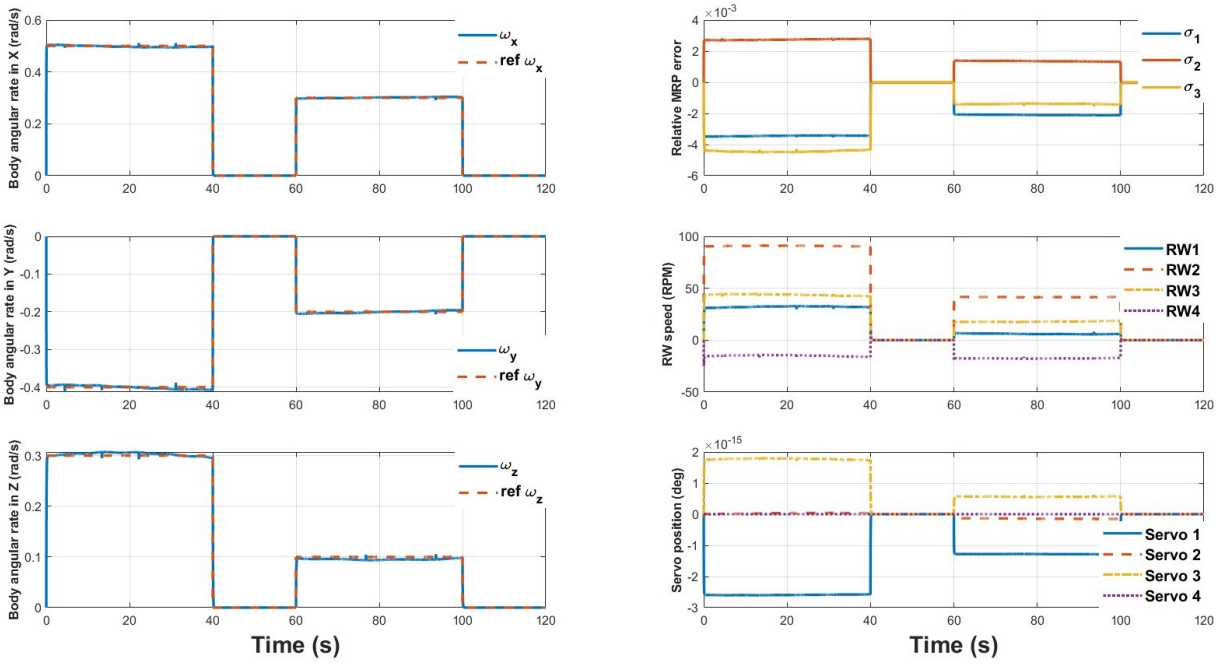

Fig. 8 Attitude tracking control with each simulation aspects plotted as mentioned in VSCMG mode using MPC control.

energy usage having the input and output rates maintained optimally within its bounds. The experimental validation in the simulator with the proposed controller will be performed in future work. The particular hardware setup described in this paper is under development, and the experimental findings will be reported soon.

References

[1] Kim, B., Velenis, E., Kriengsiri, P., and Tsiotras, P., "Designing a low-cost spacecraft simulator," *IEEE Control Systems Magazine*, Vol. 23, No. 4, 2003, pp. 26–37.

[2] Jung, D., and Tsiotras, P., "A 3-dof experimental test-bed for integrated attitude dynamics and control research," *AIAA guidance, navigation, and control conference and exhibit*, 2003, p. 5331.

[3] Jeon, S. W., and Jung, S., "Hardware-in-the-loop simulation for the reaction control system using PWM-based limit cycle analysis," *IEEE Transactions on control systems technology*, Vol. 20, No. 2, 2011, pp. 538–545.

[4] Sidi, M. J., *Spacecraft dynamics and control: a practical engineering approach*, Vol. 7, Cambridge university press, 1997.

[5] Mayne, D. Q., Rawlings, J. B., Rao, C. V., and Scokaert, P. O., "Constrained model predictive control: Stability and optimality," *Automatica*, Vol. 36, No. 6, 2000, pp. 789–814.

[6] Hegrenæs, Ø., Gravdahl, J. T., and Tøndel, P., "Spacecraft attitude control using explicit model predictive control," *Automatica*, Vol. 41, No. 12, 2005, pp. 2107–2114.

[7] Mirshams, M., and Khosrojerdi, M., "Attitude control of an underactuated spacecraft using tube-based MPC approach," *Aerospace Science and Technology*, Vol. 48, 2016, pp. 140–145.

[8] Chen, X., Steyn, W. H., Hodgart, S., and Hashida, Y., "Optimal combined reaction-wheel momentum management for earth-pointing satellites," *Journal of guidance, control, and dynamics*, Vol. 22, No. 4, 1999, pp. 543–550.

[9] Yoon, H., and Tsiotras, P., "Spacecraft adaptive attitude and power tracking with variable speed control moment gyroscopes," *Journal of Guidance, Control, and Dynamics*, Vol. 25, No. 6, 2002, pp. 1081–1090.

[10] Schaub, H., Vadali, S. R., and Junkins, J. L., "Feedback control law for variable speed control moment gyros," *The Journal of the astronautical sciences*, Vol. 46, No. 3, 1998, pp. 307–328.